

# Crystal Structure and Magnetic Behavior of the Decamethylferrocenium and Decamethylchromocenium Salts of Bis(ethylenedithiolato)nickel, $[M(\text{Cp}^*)_2][\text{Ni}(\text{edt})_2]$ – Magnetic Anisotropy and Metamagnetic Behavior of $[\text{Fe}(\text{Cp}^*)_2][\text{Ni}(\text{edt})_2]$

Vasco da Gama,<sup>\*[a]</sup> Dulce Belo,<sup>[a]</sup> Sandra Rabaça,<sup>[a]</sup> Isabel C. Santos,<sup>[a]</sup> Helena Alves,<sup>[a]</sup> João C. Waerenborgh,<sup>[a]</sup> M. Teresa Duarte,<sup>[b]</sup> and Rui T. Henriques<sup>[b]</sup>

**Keywords:** Molecule-based magnets / Solid-state structures / Metamagnetism / Magnetic properties / Mössbauer spectroscopy

New electron-transfer salts,  $[M(\text{Cp}^*)_2][\text{Ni}(\text{edt})_2]$ , with  $M = \text{Fe}$  and  $\text{Cr}$ , were prepared and shown to be isostructural by X-ray crystallographic studies. The molecular structure of  $[\text{Ni}(\text{edt})_2]^-$  is reported here for the first time. The solid-state structure consists of an array of parallel alternating donors,  $[\text{Fe}(\text{Cp}^*)_2]^+$ , and acceptors,  $[\text{Ni}(\text{edt})_2]^-$ , ··DADADA·· stacks along [101]. At high temperatures ( $T > 50$ – $100$  K), the magnetic susceptibility obeys the Curie–Weiss expression, with the  $\theta$  values of  $-5$  and  $-6.7$  K for the Ni and Cr compounds respectively, revealing dominant AFM interactions. At low temperatures metamagnetic behavior was observed in case of  $[\text{Fe}(\text{Cp}^*)_2][\text{Ni}(\text{edt})_2]$ , with  $T_N = 4.2$  K and  $H_C = 14$  kG at 2 K, resulting from high magnetic anisotropy, due to the coexistence of strong FM DA intrachain interactions and strong AFM (DA and AA) interchain interactions. Single-crystal magnetization measurements with  $[\text{Fe}(\text{Cp}^*)_2][\text{Ni}(\text{edt})_2]$

showed that the transition from the AFM state to the FM high-field state was induced by the application of a magnetic field parallel to the stacking axis. In these compounds the AFM interchain (DA and AA) interactions play a dominant role, due to the large spin density on the periphery of the acceptor and the close AA and DA interchain contacts. Above 4.2 K the  $^{57}\text{Fe}$  Mössbauer spectra of  $[\text{Fe}(\text{Cp}^*)_2][\text{Ni}(\text{edt})_2]$  exhibit the classical low spin  $\text{Fe}^{\text{III}}$  ferrocenium singlet. Below this temperature a poorly resolved hyperfine pattern is observed (estimated hyperfine field ca. 350 kG at 3.5 K). The analysis of the spectra obtained in applied fields of 20 kG and 50 kG is consistent with a strongly anisotropic  $g$  tensor. A pronounced temperature dependence of the spectra in a field of 50 kG suggests the presence of spin-lattice relaxation effects.

## Introduction

Since the observation of bulk ferromagnetism in  $[\text{Fe}(\text{Cp}^*)_2](\text{TCNE})$ ,<sup>[1,2]</sup> substantial efforts have been devoted to the study of molecule-based magnets, in particular to electron-transfer salts based on decamethylmetallocenium donors and planar acceptors.<sup>[3,4]</sup> Bulk ferromagnetism was observed in several other similar metallocenium-based electron-transfer salts,<sup>[4]</sup> and a study of the structure-magnetic property relationship revealed the need for a 1D  $\text{D}^+\text{A}^-\text{D}^+\text{A}^-\text{D}^+\text{A}^-$  chain structure to achieve ferromagnetic coupling and bulk ferromagnetism.<sup>[4]</sup>

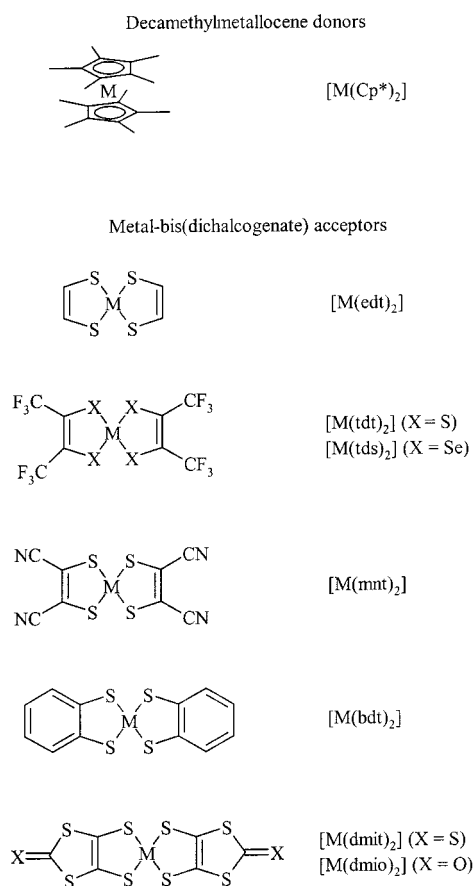
Following the extensive use of conjugated polynitriles like TCNE and TCNQ as acceptors, planar monoanionic  $S = 1/2$  metal–bis(dichalcogenate) complexes,  $[M(\text{X}_2\text{C}_2\text{R}_2)_2]^-$  ( $M = \text{Ni}, \text{Pd}$  and  $\text{Pt}$ ;  $\text{X} = \text{S}, \text{Se}$ ), have also been used in the preparation of molecule-based magnets. These acceptors seem particularly promising due to the presence of the peri-

pheral heteroatoms, which are expected to favor the existence of extended magnetic interactions, thus giving rise to stronger magnetic interactions and higher magnetic ordering temperatures. However, up to now, in most cases the structural motifs obtained differ from the simple alternating form mentioned above, and were observed only in the decamethylmetallocenium  $[M(\text{tdt})_2]^-$ ,<sup>[5,6]</sup> and  $[M(\text{tds})_2]^-$ <sup>[7]</sup> salts. We believe this is due to the dimensions of the complexes, as in this case, in spite the bulky  $\text{CF}_3$  group, the acceptors and the  $\text{Me}_5\text{C}_5$  ligand of the donor have comparable dimensions and are quite suitable for the simple alternating chain motif. In the salts with other dithiolate complexes, the larger R groups lead to larger axial dimensions, as with  $[M(\text{mnt})_2]^-$ ,<sup>[5]</sup>  $[M(\text{bdt})_2]^-$ ,<sup>[8]</sup>  $[M(\text{dmit})_2]^-$ ,<sup>[9,10]</sup> and  $[M(\text{dmio})_2]^-$ ,<sup>[10,11]</sup> which show structural motifs where the acceptors, or face to face pairs of acceptors, alternate with side by side pairs of donors (Scheme 1).

As the structural aspect seems to be rather significant in determining the magnetic properties of these types of molecular materials, in order to obtain the desired 1D  $\text{D}^+\text{A}^-\text{D}^+\text{A}^-\text{D}^+\text{A}^-$  chain structure motif, we decided to study the electron-transfer salts based on decamethylmetallocenium cations and the anionic complex  $[\text{Ni}(\text{edt})_2]^-$ , for which some preliminary results were reported.<sup>[8]</sup> This is the smaller dithiolene complex and in this case the S and C

<sup>[a]</sup> Dep. de Química, Instituto Tecnológico e Nuclear, Est. Nacional 10, 2686-953 Sacavém, Portugal  
Fax: (internat.) + 351-21/994-1455  
E-mail: vascog@itn1.itn.pt

<sup>[b]</sup> Dep. Eng. Química, Instituto Superior Técnico, Av. Rovisco Pais, 1049-001 Lisboa, Portugal  
Fax: (internat.) + 351-21/846-4455  
E-mail: teresa.duarte@ist.utl.pt



Scheme 1

atoms from the ligand are quite to interact with the atoms from neighboring molecules, and particularly strong intra- and interchain magnetic interactions are predicted for these salts.

The first model to achieve some consensus in the interpretation of the magnetic properties of this type of molecular materials was an extended version of McConnell's configuration interaction (CI) mechanism,<sup>[12]</sup> often designated as the McConnell II mechanism. However, the theoretical criticism and observation of FM in [Cr(Cp\*)<sub>2</sub>]<sup>+</sup>-based compounds,<sup>[13,14]</sup> in contradiction with the predictions of the McConnell II mechanism (AFM coupling) led to the appearance of alternative mechanisms, such as a more complex version of the McConnell II mechanism<sup>[15]</sup> and a model based on the molecular spin polarization effect,<sup>[3]</sup> designated as the McConnell I mechanism, which agreed quite well with the experimental observations. However, the recent report of a new series of compounds, [M(Cp\*)<sub>2</sub>]-[Ni(tds)<sub>2</sub>] (M = Fe, Mn, Cr),<sup>[7]</sup> where the magnetic coupling is compatible with the predictions of the simple version of the McConnell II mechanism, and in contradiction with the McConnell I mechanism, which has been by far the most widely used tool for dealing with magnetic coupling and ordering in molecular magnetic materials, clearly indicates the need to reexamine the model. The study of the series of electron-transfer salts [M(Cp\*)<sub>2</sub>][Ni(edt)<sub>2</sub>] (M = Fe, Mn, Cr) and, in particular, the nature of the magnetic coupling

in the different compounds of the series is also expected to contribute to the debate regarding the mechanism of the intra- and intermolecular magnetic interactions in the decamethylmetallocenium-based salts.

## Results and Discussion

### Synthesis

The compounds [M(Cp\*)<sub>2</sub>][Ni(edt)<sub>2</sub>], M = Fe (**1**) and Cr (**2**), were prepared by the same procedure: saturated equimolar solutions of [Fe(Cp\*)<sub>2</sub>]BF<sub>4</sub><sup>[12]</sup> or [Cr(Cp\*)<sub>2</sub>]PF<sub>6</sub><sup>[16]</sup> and (Et<sub>4</sub>N)[Ni(edt)<sub>2</sub>]<sup>[17]</sup> in acetonitrile were combined and the resulting compounds precipitated on standing. Dark brownish, needle-shaped crystals were collected by filtration. The preparation of [Mn(Cp\*)<sub>2</sub>][Ni(edt)<sub>2</sub>] was also attempted by a similar method, but in this case a dark powder was obtained with an elemental analysis indicative of probable decomposition during the synthesis.

### Crystal Structure

It was possible to determine the X-ray crystal structure of **1**, while in the case of compound **2**, it was only possible to determine the cell parameters due to the poor quality of the crystals, showing that **1** and **2** are isostructural. Crystal and experimental data are summarized in Table 1.

Table 1. Crystallographic data for compounds **1** and **2**

|  | <b>1</b>   | <b>2</b> <sup>[a]</sup>  |
|--|--|--|
| Empirical formula  | C <sub>24</sub> H <sub>34</sub> FeNiS <sub>4</sub>                                   | C <sub>24</sub> H <sub>34</sub> CrNiS <sub>4</sub>                               |
| Molecular mass   | 565.32   | 561.47   |
| Crystal system   | monoclinic   | monoclinic   |
| Space group  | C2/m   | C2/m   |
| Lattice constants [Å, °]                                       | <i>a</i> = 13.319(2)<br><i>b</i> = 13.698(8)<br><i>c</i> = 8.719(1)<br>β = 125.06(1) | <i>a</i> = 13.44(2)<br><i>b</i> = 13.66(2)<br><i>c</i> = 8.96(2)<br>β = 124.2(2) |
| Volume [Å <sup>3</sup> ]                                       | 1302.1(8)  | 1320(3)  |
| <i>Z</i>   | 2  | 2  |
| Density (calcd.) [Mg/m <sup>3</sup> ]                          | 1.442  | 1.413  |
| Abs. coefficient [mm <sup>-1</sup> ]                           | 1.611  |  |
| <i>F</i> (000)   | 592  |  |
| θ range [°]  | 2.39–27.99   |  |
| Index range ( <i>h,k,l</i> )                                   | –17/0, –18/1, –9/11  |  |
| Scan type  | ω-2θ   |  |
| Program data collection  | CAD4   |  |
| Data reduction   | Molen  |  |
| No. of collected refl.   | 1847   |  |
| No. of unique refl.  | 1649 ( <i>R</i> <sub>int</sub> = 0.052)  |  |
| No. of used refl./param.                                       | 1647/77  |  |
| Absorption correction  | ψ scans  |  |
| Transm.: max., min.  | 0.9994, 0.8655   |  |
| Structure refinement   | Full-matrix least squares on <i>F</i> <sup>2</sup>                                   |  |
| <i>S</i> on <i>F</i> <sup>2</sup>                              | 1.124  |  |
| <i>R</i> , <i>wR</i> <sub>2</sub> [ <i>I</i> > 2σ( <i>I</i> )] | 0.0536, 0.1028   |  |
| Δρ: max., min. [e/Å <sup>3</sup> ]                             | 0.325, –0.31   |  |

<sup>[a]</sup> Only the unit cell parameters were determined.

The monoclinic unit cell of **1** comprises unique cation and anion molecules. For [Ni(edt)<sub>2</sub>]<sup>•–</sup>, whose structure is reported here for the first time, the atom labeling, selected

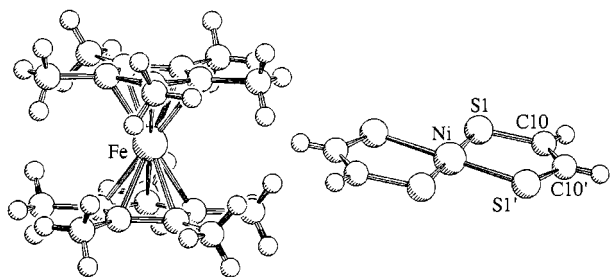


Figure 1. Perspective view of the molecular structure of **1** showing the numbering scheme for  $[\text{Ni}(\text{edt})_2]^-$ ; the primed and unprimed atoms are related by a mirror plane; selected bond lengths [Å] and angles [°]: Ni–S(1) 2.140(2), S(1)–C(10) 1.707(8), C(10)–C(10') 1.32(2); S(1)–Ni–S(1') 91.40(13), Ni–S(1)–C(10) 103.6(3), S(1)–C(10)–C(10') 120.7(3)

bond lengths and angles are given in Figure 1. This radical anion shows a  $D_{2h}$  local symmetry, is planar and the Ni–S, S–C, and C–C distances, 2.140(2), 1.707(8), and 1.32(2) Å, 2 are in good agreement with values found in other square-planar  $\text{Ni}^{\text{III}}$  dithiolate complexes.<sup>[18]</sup> The C–C distance in  $[\text{Ni}(\text{edt})_2]^-$  is relatively short when compared with the observed values in other complexes, such as  $[\text{Ni}(\text{tdt})_2]^-$ ,  $[\text{Ni}(\text{mnt})_2]^-$ , and  $[\text{Ni}(\text{bdt})_2]^-$ , 1.40(2), 1.352(8), and 1.404(2) Å, respectively.<sup>[18]</sup> This suggests the existence of a larger charge density on the C atoms for  $[\text{Ni}(\text{edt})_2]^-$ . Preliminary data for the crystal structure of the neutral  $\text{Ni}^{\text{IV}}$  complex,  $[\text{Ni}(\text{edt})_2]^0$ ,<sup>[19]</sup> revealed shorter M–S and S–C distances, 2.100 and 1.687(5) Å, along with a larger C–C distance, 1.358(7) Å, which is consistent with the antibonding nature of the Ni–S and S–C interactions and the bonding nature of the C–C interaction.<sup>[20]</sup> The  $[\text{Fe}(\text{Cp}^*)_2]^{\bullet+}$  radical cation has a  $C_5$  local symmetry and the two  $C_5$  rings show a staggered conformation, which is similar to those observed for a large number of salts with other acceptors.<sup>[5,12]</sup> The average Fe–C, C–C, and C–Me distances, 2.091(6), 1.416(8), and 1.502(9) Å, are in good agreement with the values observed for those salts.<sup>[5,12]</sup>

Similarly to the structures of the isostructural salts  $[\text{M}(\text{Cp}^*)_2][\text{M}'(\text{tdt})_2]$  (with  $\text{M} = \text{Fe}$ ,  $\text{M}' = \text{Ni}^{[5]}$  and  $\text{M} = \text{Mn}$ ,  $\text{M}' = \text{Ni}$ , Pd, Pt<sup>[6]</sup>), in the case of **1** the crystal structure consists of a parallel arrangement of 1D chains of alternate radical donors (D),  $[\text{Fe}(\text{Cp}^*)_2]^{\bullet+}$ , and acceptors (A),  $[\text{Ni}(\text{edt})_2]^-$ , DADADA, where the stacking axis corresponds to [101]. The intrachain Fe–Ni distance is 5.477 Å, as shown in Figure 2(a). Unlike the series  $[\text{M}(\text{Cp}^*)_2][\text{M}'(\text{tdt})_2]$ , where no interionic short contacts were found, in the structure of **1** intrachain short contacts between the nickel and one of the carbon atoms from the cyclopentadienyl ring were observed, with a Ni–C distance of 3.678 Å, as illustrated in Figure 2 (a). The angle between the stacking axis and the  $C_5$  ring from  $[\text{Fe}(\text{Cp}^*)_2]^{\bullet+}$  is 79.69°. The angle between the  $\text{NiS}_4$  plane of the radical anions and the stacking axis is 78.63°. The dihedral angle between the  $C_5$  ring and the  $\text{NiS}_4$  plane is 1.07° with a distance between the two planes of 2.984 Å. The existence of the short intrachain D–A contacts in this compound is expected to lead to a significantly stronger intrachain FM coupling than is observed in the case of the  $[\text{M}(\text{Cp}^*)_2][\text{M}'(\text{tdt})_2]$  series.

In the unit cell there are four distinct chains, shown in Figure 2 (b), displaying three unique interchain arrangements, I–II and II–IV, which are out-of-registry,<sup>[4]</sup> and I–III that has an in-registry<sup>[4]</sup> arrangement. The intrachain separations are 8.017, 8.678, and 13.698 Å, for the I–II, II–IV, and I–III pairs, respectively. Figure 3 shows these arrangements, along with the shortest distances between the metal centers from different chains and the closest interchain, interionic contacts (in italics). For the out-of-registry pair I–II, the shortest interchain MM distances are 8.119 (FeNi), 9.553 and 10.029 Å (FeFe or NiNi). In the case of the out-of-registry pair II–IV the shortest interchain MM separations are 8.720 (FeFe or NiNi), 9.835 and 10.740 Å (Fe Ni). For the in-registry pair I–III the

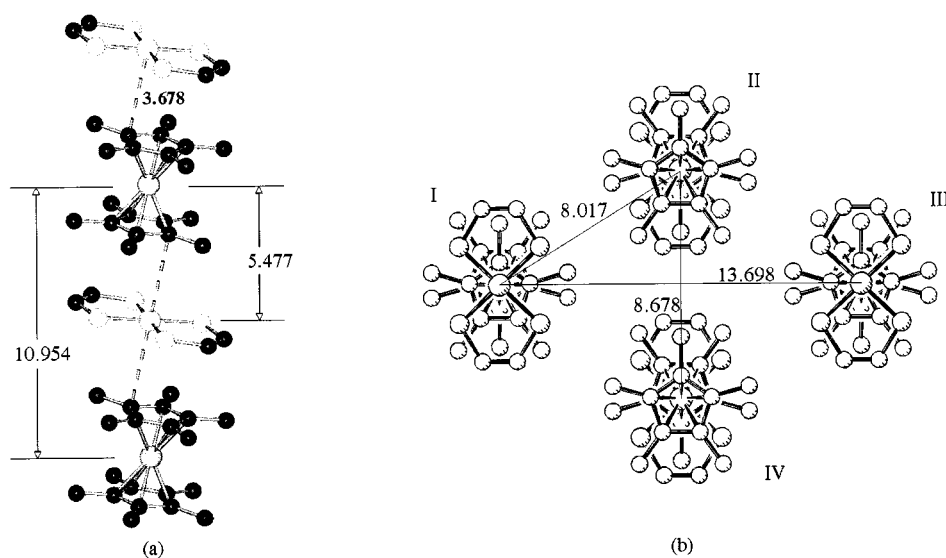


Figure 2. (a) 1D DADADA chain in **1**, the thick dotted lines represent the intrachain Ni–C short contacts, 3.678 Å; (b) view normal to the chains (along [101]), showing the four unique chains, I, II, III, IV for **1** (hydrogen atoms were omitted for clarity)

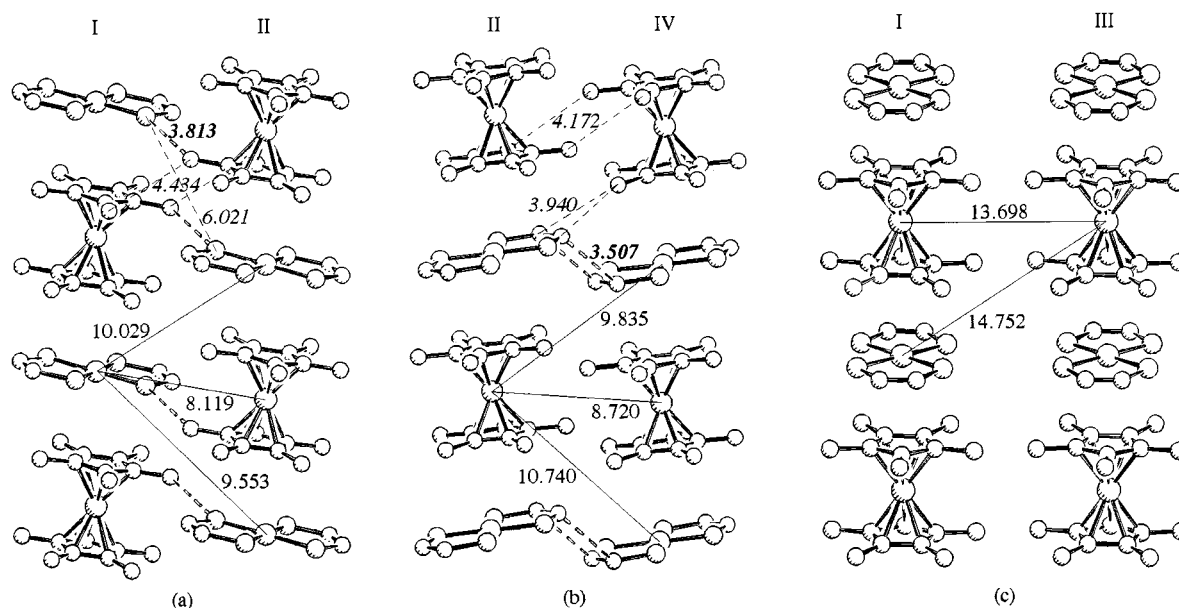


Figure 3. (a), (b) Out-of-registry arrangement of chains I–II and II–IV, respectively; (c) in-registry arrangement of chains I–III; the solid lines show the closest interchain M–M distances and the dashed lines the closest interchain interionic distances (hydrogen atoms were omitted for clarity)

shorter interchain FeFe (or NiNi) distance is 13.698 Å and the shorter FeNi distance is 14.752 Å.

Since the magnetic ordering is a bulk property, the interchain interactions are as important as the intrachain interactions and this information is essential in order to understand the spin-spin interactions that dominate the magnetic behavior. For compound **1**, although no interchain contacts shorter than the sum of the van der Waals radii were detected, relatively short DA and AA interionic interchain distances were observed in the cases of the arrangements I–II and II–IV, respectively. In the I–II pair the shortest distance (3.813 Å) corresponds to SC contacts, from a sulfur atom of the acceptor and a C from one of the methyl groups of the Me<sub>5</sub>C<sub>5</sub> fragment, as shown in Figure 3 (a). In the II–IV pair, the shortest interionic interchain distance (3.507 Å) corresponds to CC contacts from the acceptors, as shown in Figure 3 (b).

As in the case of the intrachain interactions, the interchain coupling must also be considerably stronger in **1** than in the [M(Cp\*)<sub>2</sub>][M'(tdt)<sub>2</sub>] compounds, as in these compounds the presence of the relatively bulky CF<sub>3</sub> groups isolate the S–C=C–S portion of the ligand, where most (50–70%) of the spin density must reside,<sup>[21]</sup> from the ions in the neighboring chains. In compound **1** the atoms of the S–C=C–S fragment are free to interact with the ions in the neighboring chains, and as shown in Figure 3, the S and C atoms are relatively close to atoms from different chains. The interchain spin interactions, due to the CC contacts from the acceptors, are expected to be of particular importance, since a considerable spin density must reside on those atoms. Additionally, in this case the interactions are predicted to be AFM in nature since the spin density on both atoms must have the same parity.

### Magnetic Properties

Magnetization measurements with polycrystalline samples of **1** were obtained between 2 and 300 K using the Faraday method. The magnetic susceptibility,  $\chi$ , follows the Curie–Weiss expression,  $\chi_M = C/(T - \theta)$ , between 100 and 300 K, with  $\theta = -5 \pm 4$  K. From measurements made with three different samples considerable scatter was observed in the room-temperature effective moment,  $\mu_{\text{eff}}$ , and values ranging from 3.15 to 3.95  $\mu_B$  were obtained. This can be attributed to orientation effects due to the applied field, together with the large anisotropy of the  $g$  value of [Fe(Cp\*)<sub>2</sub>]<sup>+</sup>, where  $g_{\parallel} = 4.4$ ,  $g_{\perp} = 1.3$  and  $\langle g \rangle = 2.8$ .<sup>[12]</sup> In this case, assuming independent spins and a random orientation and a  $g$  value of 2.06 for the acceptor,<sup>[22]</sup> a value of 3.0  $\mu_B$  for  $\mu_{\text{eff}}$  is predicted, but orientation effects could give rise to values as large as 4.2  $\mu_B$ . At low temperatures, the magnetic susceptibility was observed to show a considerable field dependence. The temperature dependence of the product,  $\chi_T$ , for two measurements with the same sample of **1** is shown in Figure 4. The solid circles correspond to a ZFC measurement with an applied field of 10 kG, and fit (dotted line) Curie–Weiss behavior, with  $\theta = -7.8$  K. The open circles refer to data obtained at 5 kG, where the alignment of the sample was induced through the application of a 50-kG magnetic field, the fit of the results with the Curie–Weiss expression (solid line) gave a  $\theta$  value of  $-1.6$  K. The different  $\theta$  values observed for the random and field-oriented measurements suggest the existence of strong anisotropy in the magnetic coupling in the case of **1**.

In the case of compound **2**, the magnetic susceptibility data were obtained using a Faraday magnetometer, with a freshly prepared polycrystalline sample. The magnetic sus-

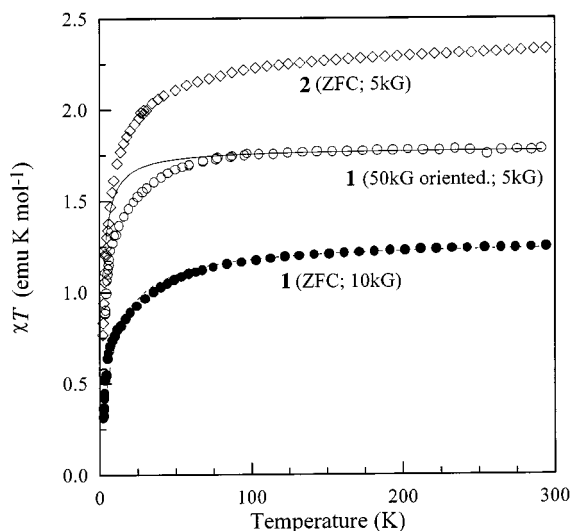


Figure 4.  $\chi_T$  temperature dependence for compounds **1** (circles) and **2** (diamonds); in the case of **1**, the closed circles refer to a ZFC measurement at 10 kG and the open circles refer to a measurement at 5 kG, where the sample was previously subjected to a 50-kG applied field, at 2 K.

ceptibility,  $\chi$ , relative to a ZFC measurement with an applied field of 5 kG, between 50 and 300 K follows the Curie–Weiss law, with  $\theta = -6.7$  K. The  $\chi_T$  temperature dependence for **2** is shown in Figure 4 (diamonds). The observed room-temperature effective moment ( $\mu_{\text{eff}} = 4.31 \mu_{\text{B}}$ ) is in good agreement with the expected value,  $4.24 \mu_{\text{B}}$ , calculated for two non-interacting spins, with  $S = 1/2$  and  $S = 3/2$ , assuming that the  $g$  values of the donor and the acceptor are 2.0<sup>[16]</sup> and 2.06,<sup>[22]</sup> respectively. Previous measurements showed unexpectedly low values for the Curie constant, which can be attributed to partial decomposition of the sample. The observed values for the magnetization field dependence at 2 K in the case of this compound are considerably lower to those calculated from the Brillouin function, indicating a strong AFM coupling. Unexpectedly, this compound was observed to be EPR-silent, which may be due to the existence of a different phase of this compound, possibly neutral. This would also explain the lower values of the magnetic susceptibility observed in previous measurements.

In order to investigate the field-dependent behavior of **1** observed at low temperatures, a series of measurements of the field cooled magnetization temperature dependence at different values of the applied field were made, as shown in Figure 5. From these experiments it was possible to observe the existence of a field-induced transition. As the sample is cooled below 30 K, in a field of 2 kG (Figure 5 – diamonds)  $\chi$  increases, reaches a maximum at 4.1 K and decreases significantly at lower temperatures, indicating that an AFM phase transition occurs. With an applied field of 10 kG (Figure 5 – circles), the behavior is similar, but there is small shift in the maximum to lower temperatures (3.9 K), at higher applied fields the maximum broadens and shifts to lower temperatures. At fields higher than 20 kG this maximum is no longer observed, suggesting that a field-induced transition occurs. Dynamic susceptibility measure-

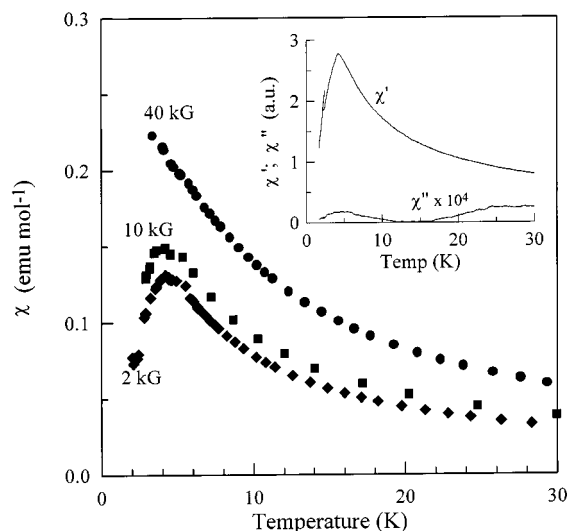


Figure 5.  $\chi$  temperature dependence for **1**, with applied fields of 2 kG (diamonds), 10 kG (squares) and 40 kG (circles); the inset shows the  $\chi'$  and  $\chi''$  temperature dependence

ments enabled the determination of the Néel temperature,  $T_N = 4.2$  K, which corresponds to a peak observed on both the in-phase,  $\chi'$  and the out-of-phase,  $\chi''$ , components, as shown in the inset of Figure 5.

The field dependence of the magnetization at 2, 3, and 6 K for compound **1** is shown in Figure 6 for a polycrystal-

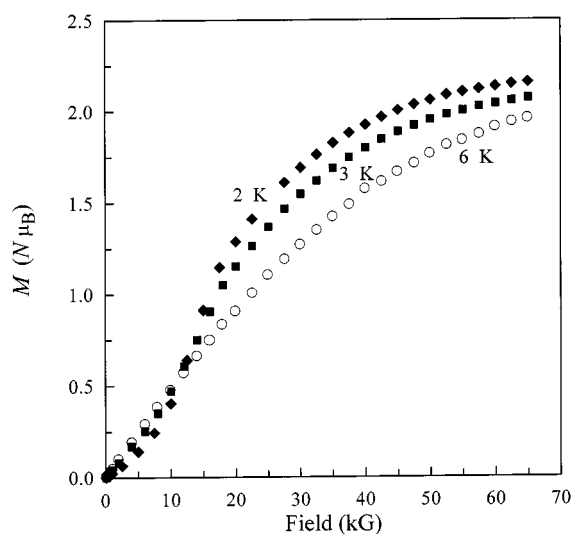


Figure 6. Magnetization field dependence for **1**, at 2, 3, and 6 K

line, pre-aligned sample. Below  $T_N$ , the curves exhibit sigmoidal behavior, typical of metamagnetism. At low fields, the magnetization increases slowly with the field and, at fields on the order of 5 kG, the increase is accentuated, showing an upward curvature. At fields in the order of 12–15 kG, the magnetization is nearly linearly dependent on the field and for higher fields a downward curvature is observed. This sigmoidal behavior is more pronounced at lower temperatures and, at fixed temperatures, it was observed to be more pronounced for previously aligned samples than nearly fixed, randomly oriented samples. For

this field-induced transition, at 2 K, the critical field, defined as the value of the field where  $dM/dH$  shows a maximum, is  $H_C = 14$  kG. No hysteresis was observed in the isothermals, as expected for a metamagnetic transition. This behavior is very similar to that observed in other highly anisotropic compounds, such as the electron-transfer salts  $[\text{Mn}(\text{Cp}^*)_2][\text{M}(\text{tdt})_2]$  ( $M = \text{Ni}, \text{Pd}, \text{Pt}$ )<sup>[6]</sup> or compounds with extended covalent networks such as  $\text{M}(\text{pyr})_2\text{Cl}_2$  ( $M = \text{Co}, \text{Fe}, \text{Ni}$ ).<sup>[23]</sup>

In order to study the magnetic anisotropy of compound **1**, single-crystal measurements were performed on a SQUID magnetometer. Due to the needle-shaped form of the crystals two configurations were used for these measurements, one (L) with the applied field parallel to the axis of the crystals, which corresponds to  $a^*$  and is relatively close to the stacking direction [101], making an angle of  $5.65^\circ$ . In a second configuration (T), the field was applied along a random direction in the plane perpendicular to  $a^*$ .

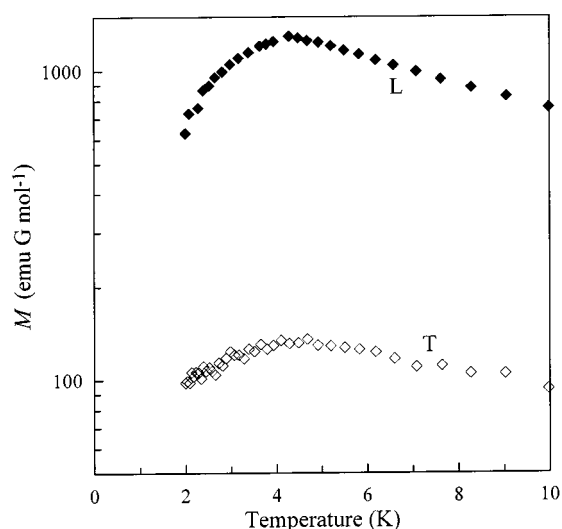


Figure 7. Single-crystal magnetization temperature dependence for **1** with an applied field of 5 kG, parallel (solid symbols) and perpendicular (open symbols) to the crystal axis

Figure 7 shows the magnetization temperature dependence for the two configurations, with an applied field of 5 kG. Crystals of 70 and 75  $\mu\text{g}$  were used in L and T configurations, respectively, the results for configuration L are represented by the closed symbols and for T by the open symbols. The magnetization temperature dependence observed for both configurations is qualitatively similar, with a maximum at ca. 4.5 K, indicating the existence of AFM transitions in both configurations. The values relative to the L configuration are almost one order of magnitude higher than the ones from the T configuration, which is attributed essentially to the anisotropy in the  $g$  value of the donor.

In the case of the L configuration, at 2 K, the single-crystal magnetization field dependence is consistent with

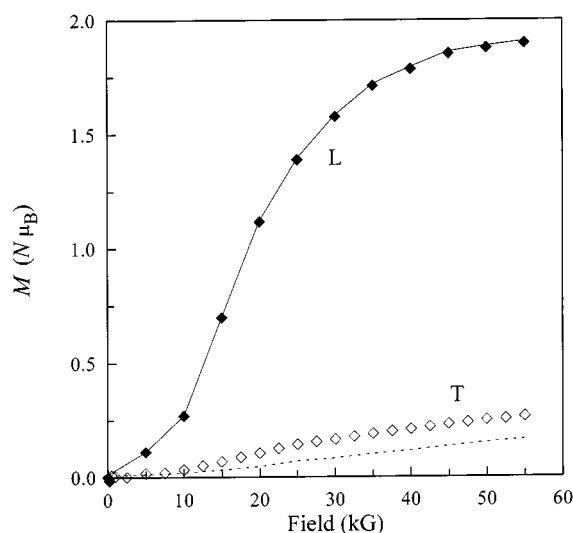


Figure 8. Single-crystal magnetization field dependence for **1**, at 2 K, with the applied field parallel (solid symbols) and perpendicular (open symbols) to the crystal axis; the estimated values of  $M_{\parallel}$  and  $M_{\perp}$  are represented by the solid and dashed lines, respectively

the existence of a field-induced phase transition, with a critical field of 14 kG, as indicated by the isothermal sigmoidal behavior, shown in Figure 8 (closed symbols). At 55 kG the magnetization reaches a value of  $1.95 N\mu_B$ , and is not yet saturated, which is usual in metamagnetic materials if the temperature is not much lower than  $T_N$ .<sup>[6,23]</sup> The high-field state is consistent with an FM state, where the saturation magnetization,  $M_S = g_D S_D + g_A S_A \approx 3 N\mu_B$ , with  $S_D = S_A = 1/2$ ,  $g_D = 3.95$  (a tilting of  $10^\circ$  of the axis of the donor relative to the field was considered) and  $g_A = 2.06$ . For a ferrimagnetic state the expected value for the saturation magnetization  $M_S = g_D S_D - g_A S_A \approx 0.91 N\mu_B$ , is much smaller than the values obtained for the high-field state. For the T configuration, the magnetization is much lower than in L, and, as shown by the open symbols in Figure 8, the magnetization field dependence is almost linear, as expected for an AFM.

In order to estimate the field dependence of  $M_{\parallel}$  and  $M_{\perp}$ , a mathematical treatment of the values measured along  $a^*$  ( $M^{a^*_{\parallel}}$ ), L configuration, and in the plane perpendicular to  $a^*$  ( $M^{a^*_{\perp}}$ ), T configuration, where made. For  $M_{\parallel}$  a very good agreement with  $M^{a^*_{\parallel}}$  was obtained, with a negligible deviation ( $< 2\%$ ) in comparison to the experimental error, which is in the order of 5%. The field dependence of  $M_{\parallel}$  is represented by the solid line in Figure 8. A linear field dependence was obtained for  $M_{\perp}$  (dotted line in Figure 8). Unlike the values observed for the L configuration, in this case the values of  $M^{a^*_{\perp}}$  are clearly larger than the ones obtained for  $M_{\perp}$  due to the contribution of  $M_{\parallel}$ .

The single-crystal magnetization measurements confirmed the high magnetic anisotropy of **1**. The transition from the AFM low-field state to a FM high-field state was observed to occur only with the applied field parallel to the stacking axis, which confirms the FM nature of the intrachain DA coupling and the AFM nature of the interchain interactions. The small dimensions of the crystals and air

sensitivity of **2** prevented determination of the single-crystal measurements on this compound.

The magnetic properties of **1** reveal features that are somewhat unusual among the class of highly anisotropic compounds displaying metamagnetism. The magnetic behavior of compound **1** seems to be dominated by AFM interactions, whereas in most compounds of this class the FM interactions are dominant. One other aspect is related to the magnitude of the critical field, which is particularly high in the case of compound **1**.

In order to achieve a better understanding of the magnetic behavior of compound **1**, its crystal structure and magnetic properties can be compared with those of the isostructural series  $[\text{M}(\text{Cp}^*)_2][\text{M}'(\text{tdt})_2]$ .<sup>[6]</sup> The magnetic behavior of those compounds is dominated by strong intrachain FM interactions coexisting with weak interchain AFM interactions, which in the case of the Mn compounds leads to metamagnetism. In these highly anisotropic compounds  $T_N \propto |E_{\text{intra}}E_{\text{inter}}|^{1/2}$ ,<sup>[14]</sup> where the intrachain DA interaction,  $E_{\text{intra}} \propto S_D S_A J_{\text{DA}}$ , and  $E_{\text{inter}}$  is the weaker effective interchain interaction. The absence of magnetic ordering in the case of  $[\text{Fe}(\text{Cp}^*)_2][\text{Ni}(\text{tdt})_2]$  is attributed to a lower value of  $E_{\text{intra}}$ , as the donor in this case has a smaller spin  $S = 1/2$ , while in the Mn compounds  $S = 1$ . As mentioned above, in the case of compound **1** stronger intrachain and interchain magnetic coupling are expected, which is consistent with the larger value of  $T_N = 4.2$  K as compared with the observed values for the  $[\text{Mn}(\text{Cp}^*)_2][\text{M}(\text{tdt})_2]$  compounds, 2.4, 2.8, and 2.3 K for  $M = \text{Ni}, \text{Pd},$  and  $\text{Pt}$ , respectively.<sup>[6]</sup> The interchain coupling in compound **1** is expected to be exceptionally strong, and the interchain AFM coupling must be comparable to the intrachain FM coupling, considering the apparent domination of AFM interactions observed from the magnetic susceptibility temperature dependence (Figure 4).

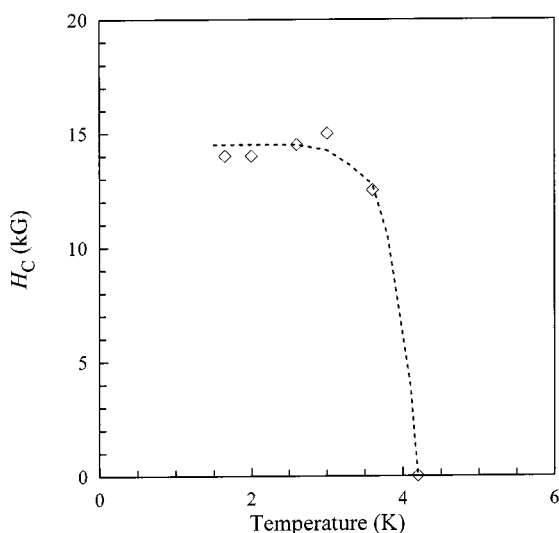


Figure 9. Critical field temperature dependence for **1**; the line represents a fit to the experimental results

A simple Ising model was used in the study of the metamagnetic transitions in the compounds  $\text{FeCl}_2 \cdot 2 \text{H}_2\text{O}$  and  $\text{CoCl}_2 \cdot 2 \text{H}_2\text{O}$ ,<sup>[24]</sup> with an intrachain and two interchain

constants, and for those compounds the metamagnetic transition fields are proportional to the interchain exchange constants. In the case of compound **1**, the high value of the observed critical field of ca. 14 kG, one order of magnitude larger than in the case of the  $[\text{Mn}(\text{Cp}^*)_2][\text{M}(\text{tdt})_2]$  compounds, can be attributed to a considerably larger interchain coupling for **1**.

As compound **2** is isostructural with **1**, it is reasonable to expect that, as observed for **1**, the magnetic behavior must be dominated by the DA intrachain and by the AA and DA interchain interactions. The magnetic susceptibility temperature dependence and the magnetization field dependence indicate that in **2** the magnetic behavior is clearly dominated by strong AFM interactions. In this compound quite strong AFM interchain interaction are expected, as in **1**, and the DA intrachain interactions must be considerable weaker, as indicated by the magnetic behavior of the  $[\text{M}(\text{Cp}^*)_2](\text{TCNE})$ , with  $M = \text{Fe}$  ( $S = 1/2$ ),  $\text{Mn}$  ( $S = 1$ ), and  $\text{Cr}$  ( $S = 3/2$ ) salts.<sup>[15]</sup> These compounds show FM ordering, with  $T_C = 4.8, 8.8,$  and  $3.1$  K for the Fe, Mn, and Cr compounds, respectively, and as in a simple mean-field model  $T_C$  is proportional to  $J$  and  $S(S+1)$ .<sup>[15]</sup> The lower value of  $T_C$  in the  $[\text{Cr}(\text{Cp}^*)_2]^+$  salt suggests that, in this case,  $J_{\text{DA}}$  is considerably weaker in relation to the other compounds, as this is the case with the higher  $S$  value. Therefore, in compound **2**, the strong AFM interchain interactions could dominate the magnetic behavior and thus it would not be possible to determine the (FM or AFM) nature of the DA intrachain interactions. Unlike the AFM DA intrachain coupling observed for  $[\text{Cr}(\text{Cp}^*)_2][\text{Ni}(\text{tds})_2]$ ,<sup>[7]</sup> in case of compound **2** the dominant interchain interactions enable discussion of the validity of the several spin-spin coupling mechanisms.

### Mössbauer Spectroscopy

Mössbauer spectra of compound **1** from 78 to 4.4 K exhibit a single line (Figure 10). The ionic form of the compound,  $[\text{Fe}(\text{Cp}^*)_2]^+[\text{Ni}(\text{edt})_2]^-$ , can be confirmed by the non-observation of quadrupole splitting along with the fact that the estimated values for the isomer shift,  $\delta = 0.48$  mm/s (relative to metallic Fe at room temperature) are typical of low-spin,  $S = 1/2$ ,  $\text{Fe}^{\text{III}}$  decamethyl ferrocenium.<sup>[25]</sup> This singlet is slightly larger at 4.4 K (half width,  $\Gamma = 0.47$  mm/s) than at 78 K ( $\Gamma = 0.38$  mm/s), but below 4.4 K the spectrum suddenly broadens and gives rise to a partially resolved hyperfine split spectrum in agreement with the magnetic ordering observed at 4.2 K in the magnetization measurements. At 3.5 K the broad sextuplet fitted to the observed spectrum (Figure 10) corresponds to a hyperfine field of ca. 350 kG.

The spectra obtained at 4.4 K with applied fields of 20 and 50 kG and at 20 K with a 50 kG applied field, shown in Figure 11, can be interpreted by the spin Hamiltonian for the  $S = 1/2$  electronic ground state [Equation (1)]

$$\mathbf{H}_{\text{NE}} = \mu_B (\mathbf{H}_{\text{ext}} \cdot \mathbf{g} \cdot \mathbf{S}_{\text{eff}}) + \mathbf{I} \cdot \mathbf{A} \cdot \mathbf{S}_{\text{eff}} + \mathbf{I} \cdot \mathbf{P} \cdot \mathbf{I} - g_N \cdot \mu_N \cdot \mathbf{H}_{\text{ext}} \cdot \mathbf{I}, \quad (1)$$

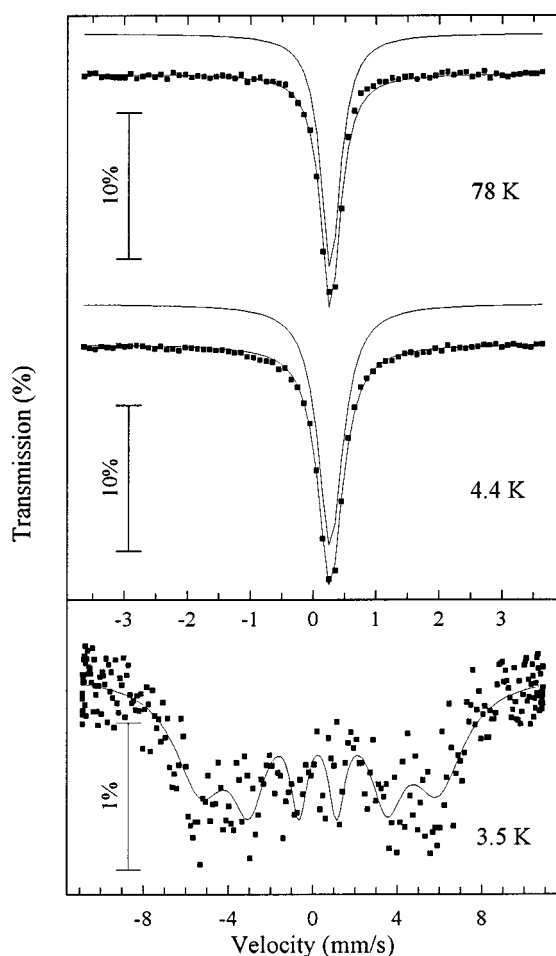


Figure 10. Mössbauer spectra of **1** obtained at 78, 4.4, and 3.5 K; the calculated functions are plotted on the experimental points; note the different velocity scale for the spectrum at 3.5 K

where  $\mathbf{g}$ ,  $\mathbf{A}$  and  $\mathbf{P}$  are tensors describing the electronic Zeeman interaction, the magnetic hyperfine interaction and the electric interaction respectively. The principal axes of  $\mathbf{g}$  and  $\mathbf{A}$  are assumed to be the same but  $\mathbf{P}$  is allowed to have different axes ( $\xi$ ,  $\psi$ ,  $\zeta$ ), which are obtained from those of  $\mathbf{g}$  or  $\mathbf{A}$  through a rotation with Euler angles  $\alpha$ ,  $\beta$ ,  $\gamma$ .  $\mathbf{I} \cdot \mathbf{P} \cdot \mathbf{I}$  may be rewritten as [Equation (2)]

$$\mathbf{I} \cdot \mathbf{P} \cdot \mathbf{I} = \frac{1}{4} eQV_{SS} \left\{ I_s^2 - \frac{1}{3} I(I+1) + \frac{\eta}{3} (I_\xi^2 - I_\psi^2) \right\}, \quad (2)$$

and we may define [Equation (3)]

$$\mathbf{H}_{\text{int}} = -\frac{\mathbf{A} \cdot \langle \mathbf{S}_{\text{eff}} \rangle}{g_N \mu_N}. \quad (3)$$

Theoretical simulations employing the above spin Hamiltonian were calculated by a modified version of the program by Münck et al.<sup>[26]</sup> Assuming fast relaxation and using  $g_{xx} = 1.3$ ,  $g_{yy} = 1.3$ , and  $g_{zz} = 4.4$ ,<sup>[12]</sup>  $\Delta E_Q = eQV_{\zeta\zeta} = -0.17$  mm/s,  $\eta = 0$ ,  $A_{xx}/(g_N \mu_N) = -110$  kG,  $A_{yy}/(g_N \mu_N) = -110$  kG, and  $A_{zz}/(g_N \mu_N) = +820$  kG, the calculated simulations are plotted on the experimental spectra (Figure 11). Non-zero values of  $\alpha$ ,  $\beta$ , and  $\gamma$  were considered but did not

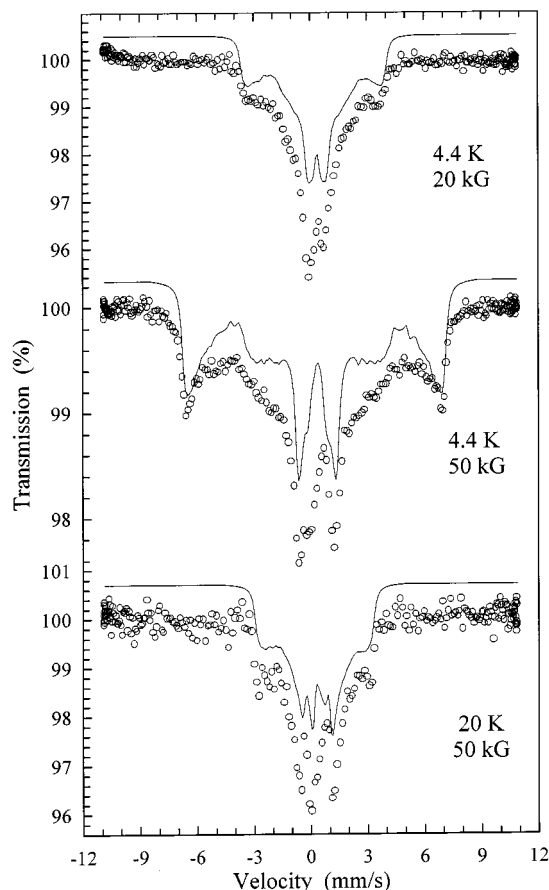


Figure 11. Mössbauer spectra of **1** with applied magnetic fields of 20 and 50 kG obtained at 4.4 K and of 50 kG at 20 K; the simulated spectra calculated using the spin Hamiltonian are also plotted slightly shifted

improve the fit of the simulation to the experimental spectra. The estimated  $\Delta E_Q$ , as well as the  $\mathbf{g}$  and  $\mathbf{A}$  values, are similar to those reported for decamethylferrocenium hexafluorophosphate.<sup>[27]</sup>

Since electronic relaxation is fast, the  $^{57}\text{Fe}$  nucleus is unable to follow the rapid fluctuations of the magnetic field  $\mathbf{H}_{\text{int}}$  due to the unpaired electrons and senses only the thermal average spin corresponding to the  $m_S = +1/2$  and  $m_S = -1/2$  levels. The magnetically split Mössbauer spectra reveal that the average  $\mathbf{H}_{\text{int}}$  is not zero. Furthermore a strong temperature and field dependence of the effective magnetic fields at the  $^{57}\text{Fe}$  nuclei is shown by the smaller splitting between the outer peaks in the spectra at 20 K with  $\mathbf{H}_{\text{ext}} = 50$  kG or at 4.4 K with  $\mathbf{H}_{\text{ext}} = 20$  kG. These observations are consistent with an appreciable difference in the Boltzmann population of spin-up and spin-down molecules and reflect the decrease in the thermal population of the excited  $m_S$  sublevel with increasing temperature and decreasing applied external magnetic field.

The spectra obtained with an applied field of 50 kG (either at 4.4 or at 20 K) bear a close resemblance to those obtained under the same experimental conditions for other decamethylferrocenium compounds characterized by a fast relaxation rate.<sup>[27]</sup> Several factors (such as relaxation rates slower than the ideal fast relaxation limit, admixtures of

electronic excited states into the ground electronic state in high magnetic fields, etc.) already mentioned by Cohn et al.<sup>[27]</sup> can influence the appearance of the Mössbauer spectra of magnetically perturbed ferrocenium cations and may explain the lack of fit between the experimental data and the simulated spectra at the Doppler velocity range around 0 mm/s. In this case significant texture effects caused by the needle shape of the crystals used in the preparation of the Mössbauer absorber should also be considered. While calculating simulated spectra, 500 different applied field directions distributed uniformly over an octant of the unit sphere associated with the **g** and **A** axes were summed, assuming a randomly oriented sample. The needle shape of the crystals is expected to cause a significant increase in the relative number of particles with the needle axis approximately perpendicular to the external field. Since the angle of the  $g_{zz}$  axis relative to the stacking direction is of the order of  $10^\circ$ , the weight of the contribution to the spectra of the cations with  $g_{zz}$  perpendicular to the applied field is larger than in the case of a randomly oriented sample.

As observed for other decamethylferrocenium salts,  $[\text{Fe}(\text{Cp}^*)_2]^+[\text{Ni}(\text{edt})_2]^-$  also shows an appreciable **g** and **A** tensor anisotropy. Furthermore, the  $A_z$  value is positive, suggesting a large orbital contribution to the hyperfine field, which along the  $z$  axis is larger in absolute value than the negative isotropic contact term. This is explained by the appreciable orbital angular momentum in the electronic ground state of this complex.<sup>[27]</sup>

## Conclusion

As predicted, the small dimensions of the acceptor,  $[\text{Ni}(\text{edt})_2]^-$ , lead to a linear chain structural motif in the electron-transfer salts,  $[\text{M}(\text{Cp}^*)_2][\text{Ni}(\text{edt})_2]$ , with  $\text{M} = \text{Ni}$  and  $\text{Cr}$ . The large spin density on the peripheral  $\text{S}-\text{C}=\text{C}-\text{S}$  fragment of the acceptor ligands and its accessibility were expected to lead to the existence of particularly strong inter- and intrachain magnetic interactions. In fact, for  $[\text{Fe}(\text{Cp}^*)_2][\text{Ni}(\text{edt})_2]$  there are strong FM intrachain interactions, due to DA intrachain short contacts coexisting with strong AFM interchain interactions, resulting from the AD and AA interchain contacts. In this compound magnetization measurements revealed the existence of a metamagnetic behavior ( $T_N = 4.2$  K and  $H_C = 14$  kG) in agreement with the high anisotropy of the magnetic coupling. Single-crystal measurements revealed that, below 4.2 K, the transition from the AFM low-field to the FM high-field state can be induced by the application of a magnetic field parallel to the stacking axis. The magnetic behavior of  $[\text{Cr}(\text{Cp}^*)_2][\text{Ni}(\text{edt})_2]$  is dominated by the strong interchain AFM interactions and in this case it was not possible to determine the exact (FM/AFM) nature of the intrachain DA interactions, which prevented a discussion of the validity of the spin-spin coupling models for these compounds.

## Experimental Section

**General Remarks:** Decamethylferrocenium tetrafluoroborate and decamethylchromocenium hexafluorophosphate were obtained

from decamethylferrocene (Aldrich) and decamethylchromocene (Strem), respectively, by literature procedures.<sup>[12,16]</sup> The  $(\text{Et}_4\text{N})[\text{Ni}(\text{edt})_2]$  salt was prepared as described in the literature.<sup>[17]</sup> Acetonitrile was distilled from  $\text{P}_2\text{O}_5$  under nitrogen, and deaerated either by successive alternate freezing and evacuation cycles or by bubbling argon through the solvent for ca. half an hour. All the syntheses were carried out under nitrogen or argon, in gloveboxes or using Schlenk techniques. – Elemental analyses were carried out with a Carlo Erba (EA 1110-CHNS-O).

**$[\text{Fe}(\text{Cp}^*)_2][\text{Ni}(\text{edt})_2]$  (1):** Dark green needle-shaped crystals of this compound were obtained by mixing  $[\text{Fe}(\text{Cp}^*)_2]\text{BF}_4$  (124 mg, 0.30 mmol) in acetonitrile (2 mL) with  $(\text{Et}_4\text{N})[\text{Ni}(\text{edt})_2]$  (111 mg, 0.30 mmol) in acetonitrile (7 mL). After standing at room temperature overnight, the crystalline product was collected by vacuum filtration in 63% yield (107 mg, 0.19 mmol). –  $\text{C}_{24}\text{H}_{34}\text{FeNiS}_4$  (565.3): calcd. C 50.99, H 6.06, S 22.68; found C 50.58, H 5.76, S 21.75. – Crystallization by slow solvent evaporation from concentrated acetonitrile or dichloromethane solutions of  $[\text{Fe}(\text{Cp}^*)_2][\text{Ni}(\text{edt})_2]$  afforded large needle-shaped crystals suitable for X-ray diffraction and single-crystal magnetic studies.

**$[\text{Cr}(\text{Cp}^*)_2][\text{Ni}(\text{edt})_2]$  (2):** The compound was prepared by the addition of  $[\text{Cr}(\text{Cp}^*)_2]\text{PF}_6$  (80 mg, 0.17 mmol) in acetonitrile (1.5 mL) to  $(\text{Et}_4\text{N})[\text{Ni}(\text{edt})_2]$  (62.6 mg, 0.17 mmol) in acetonitrile (5 mL). After standing for 2 h, brown needle-shaped crystals were collected by vacuum filtration in 49% yield (47.1 mg, 0.84 mmol). –  $\text{C}_{24}\text{H}_{34}\text{CrNiS}_4$  (561.5): calcd. C 51.34, H 6.10; found C 51.11, H 6.49. – Crystallization attempts, following the procedure described for **1**, gave small needle-shaped crystals. Partial decomposition during the crystallization was observed to occur.

**Magnetic Characterization:** Static magnetic susceptibility data of  $[\text{M}(\text{Cp}^*)_2][\text{Ni}(\text{edt})_2]$  ( $\text{M} = \text{Fe}$  and  $\text{Cr}$ ) polycrystalline samples, using Teflon sample holders, were obtained between 1.8 and 300 K using an Oxford Instruments Faraday system having a 70-kG superconducting magnet. For  $[\text{Fe}(\text{Cp}^*)_2][\text{Ni}(\text{edt})_2]$  magnetization data, between 1.5 and 300 K, were also obtained using the extraction method with an Oxford Instruments Magnetometer (MagLab System 2000), with a 120-kG superconducting magnet. Dynamic susceptibility measurements, in a zero applied static magnetic field and an alternating field of 1 G at 1 kHz, were also obtained with the MagLab system. The single-crystal magnetization measurements were obtained with a Quantum Design SQUID (MPS) magnetometer, between 2 and 10 K, with a 55-kG superconducting magnet. Magnetization measurements, in case of  $[\text{Cr}(\text{Cp}^*)_2][\text{Ni}(\text{edt})_2]$ , were also obtained with the SQUID magnetometer for polycrystalline samples, using a quartz sample holder. Susceptibility and magnetization data were corrected for contributions due to sample holder and core diamagnetism, estimated from tabulated Pascal constants. Electronic paramagnetic resonance spectra were obtained with an X-band spectrometer (Bruker ESP 300) equipped with a helium flow cryostat (Oxford ESR 300).

**Mössbauer Spectroscopy:**  $^{57}\text{Fe}$ -Mössbauer spectra were collected at 78, 4.4, and 3.5 K using a conventional spectrometer with a 50-mCi  $^{57}\text{Co}$  source in an Rh matrix and a sinusoidal velocity-vs.-time wave form. The spectrometer was calibrated with an  $\alpha$ -Fe foil. Needle-shaped crystals of **1** were mixed with perspex powder and the resulting material was pressed into a perspex sample holder in order to obtain a disk-shaped Mössbauer absorber, containing ca. 5 mg of natural Fe/cm<sup>2</sup>. Spectra with the sample in an applied external magnetic field,  $\mathbf{H}_{\text{ext}}$  (20 and 50 kG), parallel to the  $\gamma$ -ray beam, were obtained at 4.4 and 20 K using a superconducting coil. The spectra obtained at zero applied field were fitted to Lorentzian

lines using a modified version of the non-linear least-squares computer method of Stone.<sup>[28]</sup>

**X-ray Crystallographic Study:** A single crystal of **1** with approximate dimensions of  $1.4 \times 0.35 \times 0.25$  mm was used for X-ray data collection with an Enraf Nonius Cad4 diffractometer, with graphite-monochromated Mo- $K_{\alpha}$  radiation ( $\lambda = 0.71069$  Å), at room temperature. The structure was solved by direct methods using SHELXS-86<sup>[29]</sup> and refined with SHELXL-93.<sup>[30]</sup> All non-hydrogen atoms were refined anisotropically and hydrogen atoms were placed at calculated positions with isotropic temperature factors  $U(H) = 1.2U_{eq}(C)$ . All crystal and molecular representations were prepared with SCHAKAL-97.<sup>[31]</sup> The unit cell of compound **2** was determined using a single crystal with approximate dimensions of  $0.8 \times 0.15 \times 0.1$  mm with an Enraf Nonius Cad4 diffractometer (Mo- $K_{\alpha}$  radiation). However, in this case the poor quality of the crystal prevented the X-ray structure determination. A summary of the crystal data and refinement procedures is given in Table 1. Crystallographic data (excluding structure factors) for the structure(s) reported in this paper have been deposited with the Cambridge Crystallographic Data Centre as supplementary publication no. CCDC-137238. Copies of the data can be obtained free of charge on application to CCDC, 12 Union Road, Cambridge CB2 1EZ, UK [Fax: (internat.) + 44-1223/336-033; E-mail: deposit@ccdc.cam.ac.uk].

## Acknowledgments

This work was partially supported by "Fundação para a Ciência e Tecnologia" under contracts 2/2.1/QUI/203/94 and PBIC/C/2204/95 from PRAXIS XXI program.

- [1] J. S. Miller, J. C. Calabrese, A. J. Epstein, W. Bigelow, J. H. Zhang, W. M. Reiff, *J. Chem. Soc., Chem. Commun.* **1986**, 1026–1028.
- [2] S. Chittipeddi, K. R. Cromack, J. S. Miller, A. J. Epstein, *Phys. Rev. Lett.* **1987**, *58*, 2695–2698.
- [3] O. Kahn, *Molecular Magnetism*, VCH Publ., New York, **1993**, chapter 11 and references therein.
- [4] J. S. Miller, A. J. Epstein, in: *Research Frontiers in Magnetochemistry* (Ed.: C. J. O'Connor), World Scientific, Singapore, **1993**, p. 283–302, and references therein.
- [5] J. S. Miller, J. C. Calabrese, A. J. Epstein, *Inorg. Chem.* **1989**, *28*, 4230–4238.
- [6] W. E. Broderick, J. A. Thompson, B. M. Hoffman, *Inorg. Chem.* **1991**, *30*, 2958–2960.
- [7] V. Gama, S. Rabaça, C. Ramos, D. Belo, I. C. Santos, M. T. Duarte, *Mol. Cryst. Liq. Cryst.* **1999**, *335*, 81–90.
- [8] V. Gama, D. Belo, I. C. Santos, R. T. Henriques, *Mol. Cryst. Liq. Cryst.* **1997**, *306*, 17–24.
- [9] W. E. Broderick, J. A. Thompson, M. R. Godfrey, M. Sabat, B. M. Hoffman, *J. Am. Chem. Soc.* **1989**, *111*, 7656–7657.
- [10] S. Rabaça, V. Gama, D. Belo, I. C. Santos, M. T. Duarte, *Synth. Met.* **1999**, *103*, 2302–2303.
- [11] M. Fettouhi, L. Ouahab, E. Codjovi, O. Kahan, *Mol. Cryst. Liq. Cryst.* **1995**, *273*, 29–33.
- [12] J. S. Miller, J. C. Calabrese, H. Rommelmann, S. R. Chittipeddi, J. H. Zhang, W. M. Reiff, A. J. Epstein; *J. Am. Chem. Soc.* **1987**, *109*, 769–781.
- [13] D. M. Eichhorn, D. C. Skee, W. E. Broderick, B. M. Hoffman, *Inorg. Chem.* **1993**, *32*, 491–492.
- [14] W. E. Broderick, B. M. Hoffman, *J. Am. Chem. Soc.* **1991**, *113*, 6334–6335.
- [15] J. S. Miller, A. J. Epstein, *Angew. Chem. Int. Ed. Engl.* **1994**, *33*, 385–415, and references therein.
- [16] J. L. Robbins, N. Edelstein, B. Spencer, J. C. Smart, *J. Am. Chem. Soc.* **1982**, *104*, 1882–1893.
- [17] W. Schroth, J. Peschel, *Chimia* **1964**, *18*, 171–173.
- [18] C. Mahadevan, M. Seshasayee, P. Kuppusamy, P. T. Manoharan, *J. Cryst. Spectrosc. Res.* **1985**, *15*, 305–316.
- [19] [19a] K. W. Browall, T. Bursh, L. V. Interrante, J. S. Kasper, *Inorg. Chem.* **1972**, *11*, 1800–1806. – [19b] Z. S. Herman, R. F. Kirchner, G. H. Loew, U. T. Mueller-Westerhoff, A. Nazzari, M. C. Zerner, *Inorg. Chem.* **1982**, *21*, 46–56.
- [20] M. Sano, H. Adachi, H. Yamatera, *Bull. Chem. Soc. Jpn.* **1981**, *54*, 2639–2641.
- [21] W. B. Heuer, A. E. True, P. N. Swepston, B. M. Hoffman, *Inorg. Chem.* **1988**, *27*, 1474–1482.
- [22] J. A. MacLeaverty, in: *Progress in Inorganic Chemistry*, vol. 10 (Ed.: F. A. Cotton), Intersc. Publ., **1968**, p. 49–221.
- [23] S. Foner, R. B. Frankel, W. M. Reiff, B. F. Little, G. J. Long, *Solid State Commun.* **1975**, *16*, 159–161.
- [24] A. Narath, *Phys. Rev.* **1965**, *139*, A1221–A1227.
- [25] J. S. Miller, J. C. Calabrese, R. L. Harlow, D. A. Dixon, J. H. Zhang, W. M. Reiff, S. R. Chittipeddi, M. A. Selover, A. J. Epstein, *J. Am. Chem. Soc.* **1990**, *112*, 5496–5506.
- [26] E. Münck, J. L. Groves, T. A. Tumolillo, P. G. Debrunner, *Comput. Phys. Chem.* **1973**, *5*, 225–238.
- [27] M. Cohn, M. Timken, D. N. Hendrickson, *J. Am. Chem. Soc.* **1984**, *106*, 6683–6689.
- [28] J. C. Waerenborgh, F. Teixeira de Queiroz, *Research Report*, Laboratório Nacional de Engenharia e Tecnologia Industrial, Instituto de Ciências e Engenharia Nucleares, **1984**.
- [29] G. M. Sheldrick, *SHELXS-86, A Program for Crystal Structure Determination*, University of Göttingen, Germany, **1990**.
- [30] G. M. Sheldrick, *SHELXL-93, A Program for Crystal Structure Refinement*, University of Göttingen, Germany, **1993**.
- [31] E. Keller, *SCHAKAL-97, A Computer Program for the Representation of Molecular and Crystallographic Models*, Kristallographisches Institut der Universität Freiburg i. Br., Germany, **1997**.

Received December 3, 1999  
[I99422]